Asymmetry in electrical coupling between neurons alters multistable firing behavior

A. N. Pisarchik, R. Jaimes-Reátegui, and M. A. García-Vellisca

Citation: Chaos **28**, 033605 (2018); doi: 10.1063/1.5003091
View online: https://doi.org/10.1063/1.5003091
View Table of Contents: http://aip.scitation.org/toc/cha/28/3
Published by the American Institute of Physics

CHAOS 28, 033605 (2018)

Asymmetry in electrical coupling between neurons alters multistable firing behavior

A. N. Pisarchik,[1,2,a)] R. Jaimes-Reátegui,[3] and M. A. García-Vellisca[1]
[1]Center for Biomedical Technology, Technical University of Madrid, Pozuelo de Alarcon 28223, Spain
[2]Yuri Gagarin State Technical University of Saratov, Saratov 410054, Russia
[3]Centro Universitario de los Lagos, Universidad de Guadalajara, Lagos del Moreno 47460, Mexico

(Received 2 September 2017; accepted 19 January 2018; published online 2 March 2018)

The role of asymmetry in electrical synaptic connection between two neuronal oscillators is studied in the Hindmarsh-Rose model. We demonstrate that the asymmetry induces multistability in spiking dynamics of the coupled neuronal oscillators. The coexistence of at least three attractors, one chaotic and two periodic orbits, for certain coupling strengths is demonstrated with time series, phase portraits, bifurcation diagrams, basins of attraction of the coexisting states, Lyapunov exponents, and standard deviations of peak amplitudes and interspike intervals. The experimental results with analog electronic circuits are in good agreement with the results of numerical simulations. *Published by AIP Publishing.* https://doi.org/10.1063/1.5003091

An electrical synapse is a conductive link between two neurons in the form of a gap junction which allows a direct exchange of small molecules and ions between the cells. Although most gap junctions are bidirectional, some of them present an asymmetry in the electrical coupling.[1] In this paper, we show that this asymmetry can induce multistability in the coupled neural system. Since intrinsic noise in real systems can produce random switches between coexisting states, this mechanism of the intermittent behavior should be taken into account while interpreting neurophysiological data.

I. INTRODUCTION

Multistability is a widespread phenomenon in nonlinear science. The coexistence of multiple attractors has been observed in many biological models and natural systems, including biomedical systems and neuronal networks.[2] It is supposed that the brain, as a very complex system, exhibits a huge number of coexisting states and that switches between these states, induced by external stimuli and intrinsic noise, are associated with information processing and mentality.[3,4] Cooperative behavior of neurons in the neuronal network plays a crucial role in normal brain functionality.[5] It is widely accepted that functional connectivity between different brain regions and structural disconnection can be associated with some brain diseases, such as schizophrenia, epilepsy, Alzheimer's disease, tinnitus, autism, and Parkinson.[6,7] The concepts of connectivity and synchronization in neuronal networks acquire special significance when we deal with multistability.[8,9]

It is known that certain neurons in the mammalian brain are joined by electrical synapses (gap junctions) involved in several physiological mechanisms and anomalous population activity, such as epilepsy.[10,11] The gap junction creates channels through which ions and small molecules flow from one cell to the other to depolarize a more negative cell, so that the transjunction current makes the first cell less depolarized, i.e., the coupling excites one cell while inhibiting the other. Therefore, these synapses can be characterized as synchronizing rather than excitatory or inhibitory. Although in most of the papers, electrical synapses are considered to be bidirectional (see, e.g., Ref. 12 for review), there are several gap junctions which represent some asymmetry in the coupling.[1]

Bistable firing patterns were identified in many neurophysiological experiments with various species.[13–15] Recently, Kim and Jones[16] reported on their finding of bistability in firing neural dynamics in the presence of asymmetry in electrotonic coupling between the soma and dendrites. On the basis of the Morris-Lecar equations[17] and a two-compartment motor neuron model,[18] they developed a new reduced modeling approach which allowed them to find the coexistence of two different firing patterns. The authors noted that due to the simplicity of the Morris-Lecar mechanisms, they were able to find bistability only for a unique set of parameters of the asymmetric model. The open problems that still remain are whether the coexistence of attractors also occurs in asymmetrically coupled neurons, and how the asymmetry affects multistability.

To address this important issue, we consider a pair of neuronal oscillators asymmetrically coupled via an electrical synapse. Specifically, we focus on the Hindmarsh-Rose (HR) model[19] which is a simplified version of the physiological Hodgkin-Huxley model.[20] In spite of its simplicity, the HR model allows basic phenomenological description of neuron dynamics (resting, spiking, and bursting behaviors)[21–24] and reveals nonlinear mechanisms responsible for many important biological processes. In a recent paper,[25] it was shown that bistability can appear in neuronal oscillators unidirectionally coupled by electrical synapses. However, unidirectional electrical coupling is not usual in real neurons. As a rule, this kind of coupling is bidirectional, i.e., the exchange of ions and small molecules between neural cells in gap junctions occurs in both directions. In order to make our

[a)]Electronic mail: alexander.pisarchik@ctb.upm.es

model closer to reality, in this work, we explore bidirectional electrical coupling, but add an asymmetry in the coupling. Then, using the coupling strengths in two directions as control parameters, we study the system dynamics under fixed and random initial conditions. The analyses of time series, phase space, amplitude and time coherence, Lyapunov exponents, and basins of attraction allow us to reveal the coexistence of attractors in this system.

In addition, we have to note that a major part of the research on dynamics of coupled neuronal oscillators was performed by numerical simulations on neural models.[11,16,22,26–28] Significantly less attention was paid to the electronic implementation of the HR model[29] that can provide experimental evidence of theoretically predicted effects in real experimental conditions in the presence of parameter tolerances and inherent noise. Therefore, one of the aims of this research is to check whether or not the predicted theoretical findings reveal themselves in real experimental conditions.

II. NUMERICAL SIMULATIONS

We start our research with numerical simulations and then continue with experimental implementation in electronic circuits.

A. Model of coupled neural oscillators

We consider the system of two HR neurons bidirectionally coupled as follows:

$$\begin{aligned}
\dot{x}_1 &= y_1 - a x_1^3 + b x_1^2 - z_1 + I_{\text{ext}1} + \sigma_1(x_2 - x_1),\\
\dot{y}_1 &= c - d x_1^2 - y_1,\\
\dot{z}_1 &= r[s(x_1 - x_0) - z_1],\\
\dot{x}_2 &= y_2 - a x_2^3 + b x_2^2 - z_2 + I_{\text{ext}2} + \sigma_2(x_1 - x_2),\\
\dot{y}_2 &= c - d x_2^2 - y_2,\\
\dot{z}_2 &= r[s(x_2 - x_0) - z_2],
\end{aligned} \tag{1}$$

where $x_{1,2}$ are membrane potentials of neuron 1 and neuron 2, $y_{1,2}$ are recovery variables associated with a fast current of Na^+ or K^+ ions, $z_{1,2}$ are adaptation currents associated with a slow current of Ca_2^+ ions, $I_{\text{ext }1,2}$ are external input currents, $x_0 = -1.6$ is the x-component of the stable equilibrium point without input ($I_{\text{ext}} = 0$), and $0 < \sigma_{1,2} < 1$ are electrical coupling strengths used as control parameters. In the numerical simulations, we consider the following parameters: $a = 1$, $b = 3$, $c = 1$, $d = 5$, $s = 4$, and $r = 0.006$. The solitary (uncoupled) neurons oscillate periodically for small ($1.4 < I_{\text{ext}} < 2.9$) and large ($I_{\text{ext}} > 3.4$) external currents, whereas for intermediate currents ($2.9 < I_{\text{ext}} < 3.4$), they are chaotic. In this paper, we fix the currents for both neurons at $I_{\text{ext}1} = I_{\text{ext}2} = I_{\text{ext}} = 1.4$. For the considered set of the parameters, the uncoupled neurons oscillate in a periodic spiking regime.

1. Bifurcation diagrams

A simple way to reveal multistability in a dynamical system is to construct bifurcation diagrams calculated by using random initial conditions. Such diagrams for the system in Eq. (1) are shown in Fig. 1 for $\sigma_1 = 0.051$ using the coupling strength σ_2 as a control parameter.

In the bifurcation diagrams, one can distinguish the difference between dynamics of two neurons. When the coupling

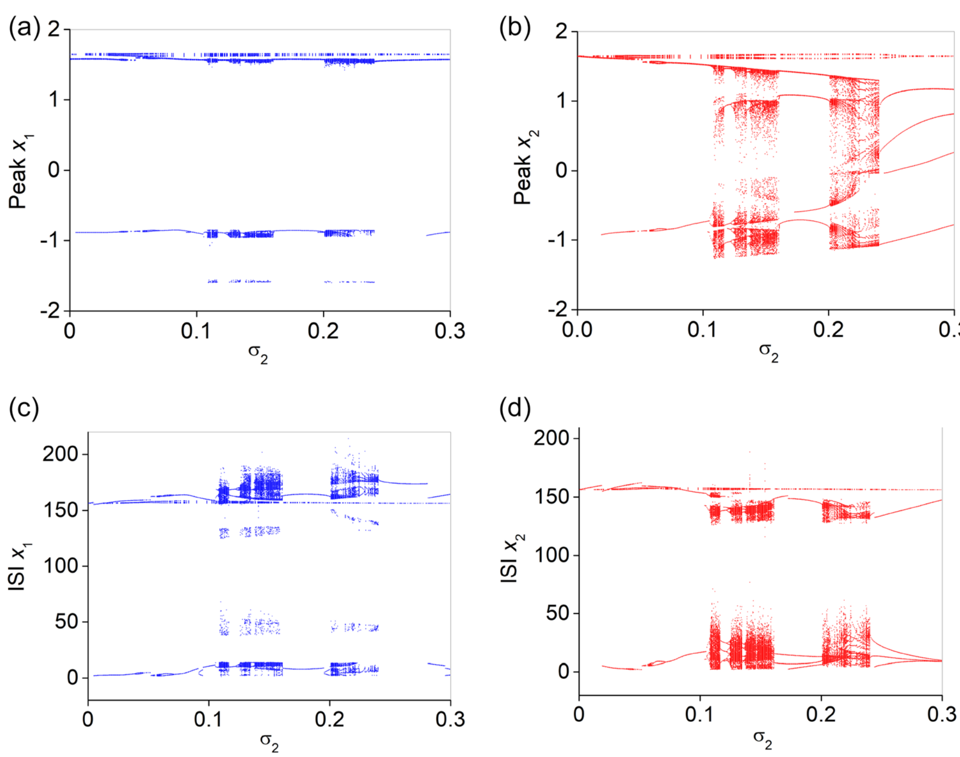

FIG. 1. Bifurcation diagrams of (a) and (b) local maxima of membrane potentials x_1 and x_2 and (c) and (d) inter-spike intervals (ISI) of membrane potentials of two coupled neurons with respect to one of the coupling strengths (σ_2), while another coupling strength is fixed ($\sigma_1 = 0.051$). The diagrams are obtained by varying randomly initial conditions.

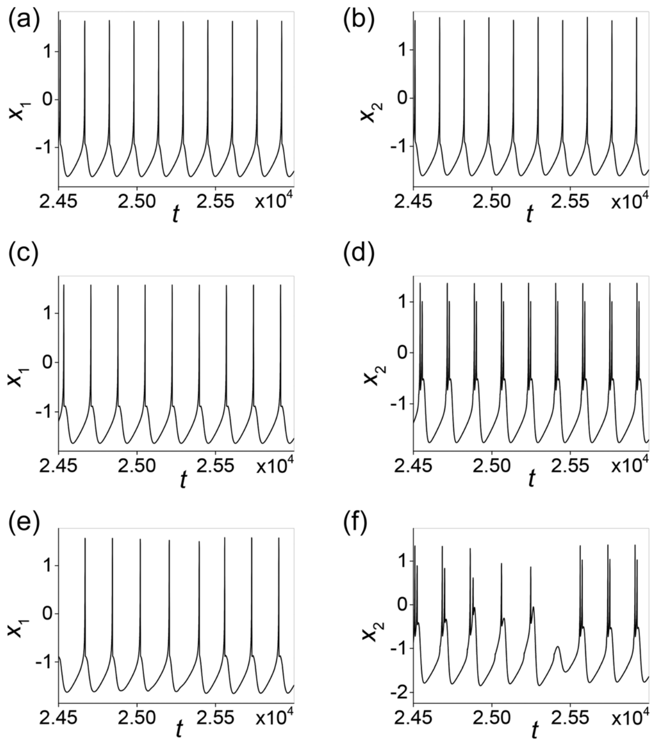

FIG. 2. Time series of membrane potentials of neuron 1 (left column) and neuron 2 (middle column) of coexisting (a)–(d) periodic and (e) and (f) chaotic attractors for $\sigma_1 = 0.051$ and $\sigma_2 = 0.2$.

σ_2 is sufficiently small, both neurons generate tonic spikes, because both couplings are too weak to change the original neural dynamics. An increase in σ_2 gives rise to other attractors, so that the system behavior becomes multistable. One can see that the bifurcation diagrams consist of several branches. The upper horizontal branch in all diagrams corresponds to a tonic spiking regime which coexists with bursting and chaotic regimes within a certain range of the control parameter. In particular, for $0.12 \lesssim \sigma_2 \lesssim 0.16$ and $0.20 \lesssim \sigma_2 \lesssim 0.24$, we find the coexistence of periodic and chaotic attractors within a certain range of the control parameter.

2. Time series

The coexistence of three spiking regimes is clearly seen in Fig. 2, where we plot the time series of membrane potentials of two coupled neuronal oscillators Eq. (1) for asymmetric coupling with $\sigma_1 = 0.051$ and $\sigma_2 = 0.2$. One can see that two periodic orbits [Figs. 2(a)–2(d)] coexist with a chaotic attractor [Figs. 2(e) and 2(f)].

The membrane potential represents a spiking behavior with either a single spike [Figs. 2(a) and 2(b)] or two spikes [Fig. 2(d)] in one burst when the system is in the periodic states or with a varying number of spikes in the chaotic regime [Fig. 2(f)]. Note that the neurons fire with the same bursting frequency; however, the number of spikes in each burst is different.

3. Phase portraits

Since the coupled system in Eq. (1) is six-dimensional, the complete phase space cannot be graphically presented. Therefore, in Fig. 3, we plot the phase portraits of three coexisting attractors in the (x_1, y_1, x_2) plane.

Since each attractor has different regularity and stability, it can be characterized by different coherence and different Lyapunov exponents. In other words, different values of the

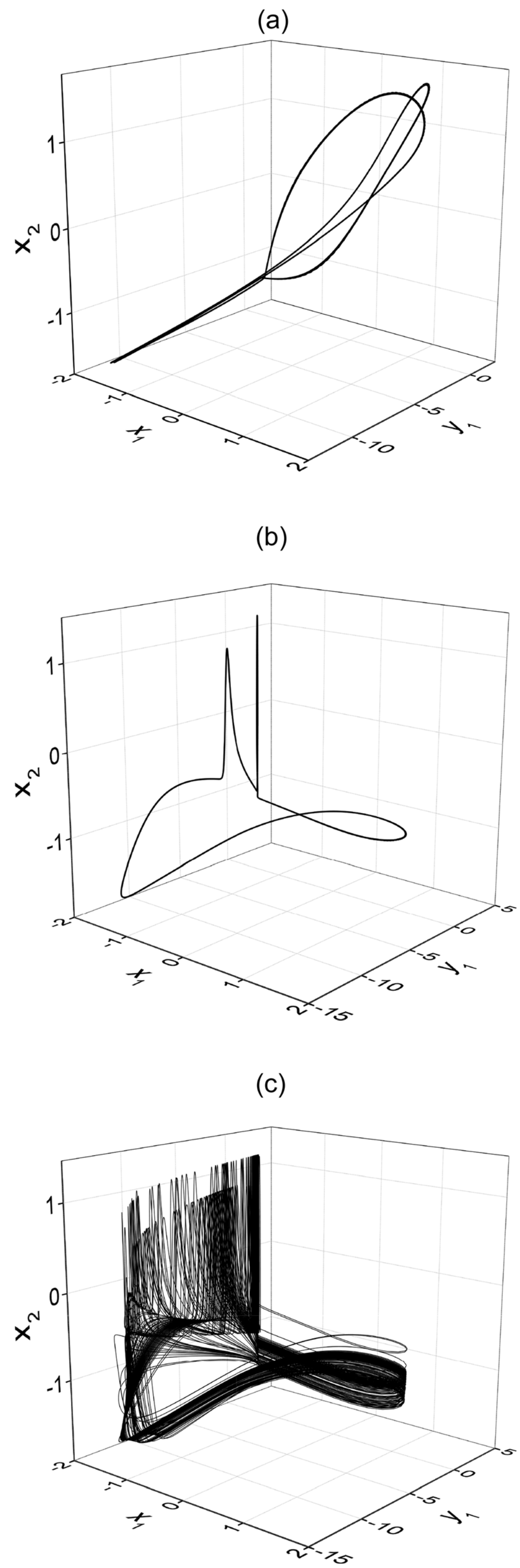

FIG. 3. Phase portraits of coexisting (a) and (b) periodic and (c) chaotic attractors for $\sigma_1 = 0.051$ and $\sigma_2 = 0.2$, in (x_1, y_1, x_2) plane.

standard deviation (SD) and Lyapunov exponents for the same parameters indicate the coexistence of different attractors. In the next two subsections, we will show how these important measure reveal multistability.

4. Coherence

Evidently, dynamical regimes with different regularity have different coherence. For instance, a periodic regime is regular and therefore coherent, whereas a chaotic or noisy regime is highly irregular and hence incoherent. As a quantitative measure of the coherence, here we will use standard deviation (SD) of the spike amplitude (amplitude coherence) and normalized standard deviation (NSD) of the inter-spike interval (ISI) (time coherence). These characteristics have been successfully used for the estimation of the coherence in coupled chaotic Rössler oscillators.[30,31]

The effect of asymmetry in coupling is clearly seen in Fig. 4, where we plot the bifurcation diagrams of SD of the local maxima [Fig. 4(a)] and NSD of the ISI [Fig. 4(b)] of the membrane potential x_2, in the parameter space of two coupling strengths. For the calculation of the local maxima, we choose the threshold value $x_1^{th} = -0.5$ to exclude small-amplitude local maxima related to the postsynaptic potential and relaxation oscillations.

Since the diagrams in Fig. 4 are constructed for fixed initial conditions, not all attractors are presented. However, the asymmetry with respect to the diagonal line in both diagrams indicates multistability, because the coupling scheme in Eq. (1) is completely symmetric. Therefore, this asymmetry is the consequence of the coexistence of different regular and irregular dynamical regimes for the same pairs of the coupling strengths σ_1 and σ_2.

5. Lyapunov exponents

Multistability in the coupled neuronal oscillators can also be revealed through the analysis of Lyapunov exponents. The leading Lyapunov exponents of the system in Eq. (1) are plotted in Fig. 5 as a function of two coupling strengths for fixed [Fig. 5(a)] and random [Fig. 5(b)] initial conditions. While in a periodic regime the largest Lyapunov exponent is zero, in a chaotic regime it is positive. One can see from Fig. 5(a) that the largest Lyapunov exponent is positive in the region of the coupling strengths $0.01 > \sigma_1 > 0.05$ and $0.10 > \sigma_2 > 0.21$. At the same time, as seen from Fig. 5(b), the exponent is positive for $0.10 > \sigma_1 > 0.21$ and $0.01 > \sigma_1 > 0.05$, symmetrically with respect to the diagonal $\sigma_1 = \sigma_2$. This means that for these control parameters the chaotic attractor coexists with periodic orbits. In other words, when the initial conditions are randomly varied, different coexisting attractors randomly arise for the same control parameters, so that the diagram is almost symmetric with respect to the diagonal [Fig. 5(b)].

B. Basins of attraction

Finally, Fig. 6 illustrates multistability with the basins of attraction of three coexisting states. As mentioned earlier, since our system is six-dimensional, we cannot visualize the complete phase space. Instead, we plot the $[y_1(0), y_2(0)]$ section of the basins of attraction, keeping other initial conditions fixed $[x_1(0) = -0.9221, z_1(0) = 1.2556, x_2(0) = -0.9127$, and $z_2(0) = 1.2603]$ for the fixed coupling strengths $\sigma_1 = 0.051$ and $\sigma_2 = 0.2$.

We should note that the periodic attractor with a single spike in one burst, shown in Figs. 2(a) and 2(b), has a larger basin of attraction (green regions) than two other coexisting attractors. One can also see that the chaotic attractor often occurs when the initial conditions for the coupled oscillators are close to each other, i.e., when $y_1(0) \approx y_2(0)$ (blue dots on the diagonal).

III. EXPERIMENTAL EVIDENCE

A. Electronic circuit

On the basis of the HR neuron model Eq. (1), we construct the electronic circuits using Kirchoff's law. The electronic scheme and general view of the Hindmarsh-Rose circuit are shown in Fig. 7. The values of the electronic components are presented in Table I.

The analog representation of the HR model Eq. (1) based on the Kirchoff's law can be written as follows:

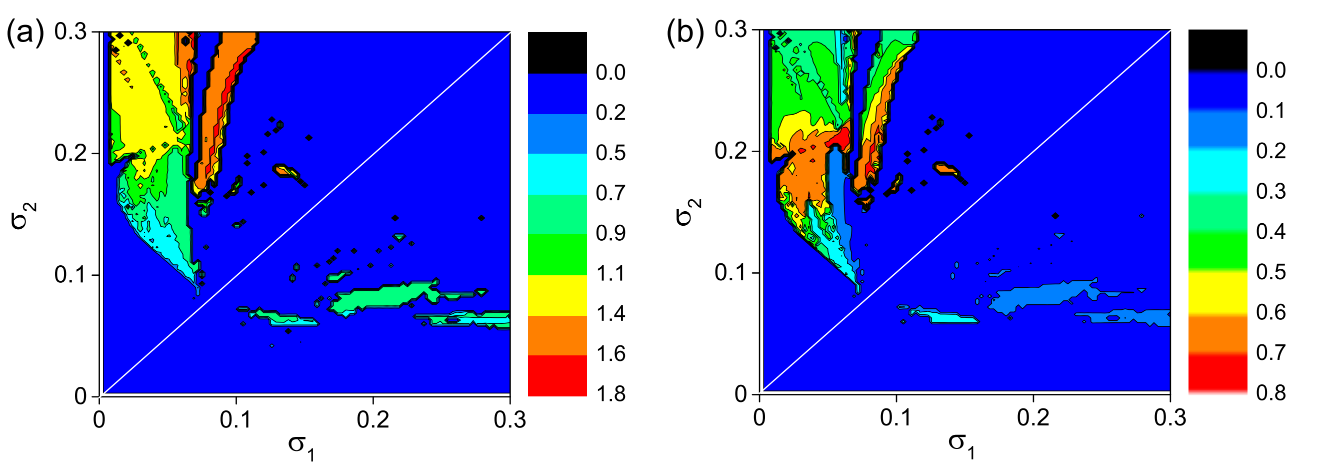

FIG. 4. Bifurcation diagrams of (a) SD of local maxima and (b) NSD of the ISI of membrane potential x_1 in the parameter space of two coupling strengths. The diagrams are obtained using fixed initial conditions. The asymmetry with respect to the diagonal lines is a signature of multistability.

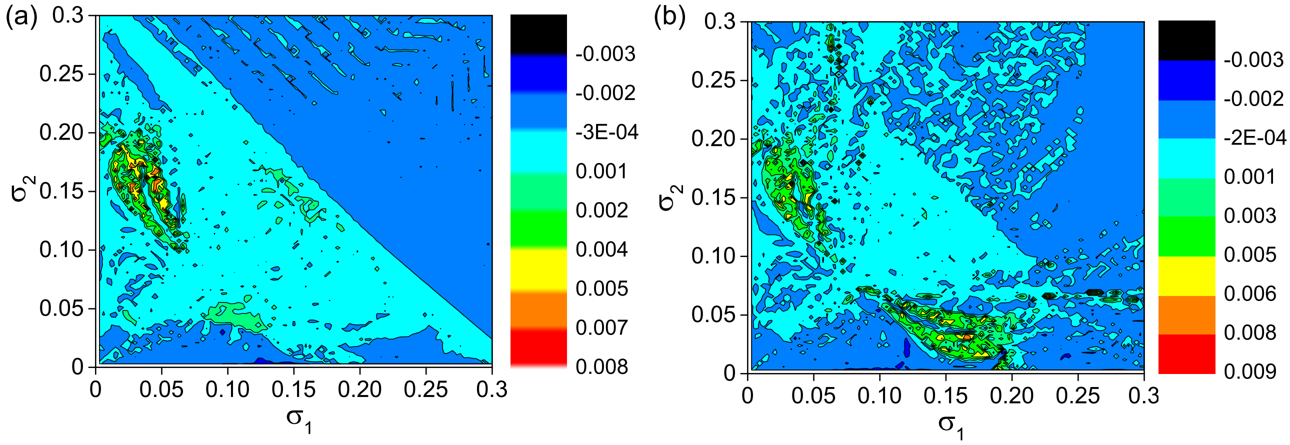

FIG. 5. Leading Lyapunov exponent as a function of coupling strengths σ_1 and σ_2 calculated for (a) fixed and (b) random initial conditions.

$$
\begin{aligned}
\dot{V}_x &= W(-AV_x^3 + BV_x^2 + CV_y - DV_z + EI_{\mathrm{ext}}),\\
\dot{V}_y &= W(F - GV_x^2 - HV_y),\\
\dot{V}_z &= WK[S(V_x - V_0) - V_z],
\end{aligned}
\tag{2}
$$

where V_x, V_y, and V_z are the voltages in the electronic circuit associated with three variables, $W = 10\,\mathrm{kHz}$ is the time-scaling frequency, and $I_{\mathrm{ext}} = V_{\mathrm{ext}}/R$ is the external current (V_{ext} and R being the external voltage and load resistance, respectively). To satisfy the theoretical model in Eq. (1), we use the following scaling coefficients: $A = 10^6\,\mathrm{V}^{-2}$, $B = 3\times10^6\,\mathrm{V}^{-1}$, $C = D = H = 10^4$, $E = 10^4\,\mathrm{V/A}$, $F = 10^4\,\mathrm{V}$, $G = 5\times10^4\,\mathrm{V}^{-1}$, $K = 50$, $S = 4$, $V_0 = 1.6\,\mathrm{V}$, and $I_{\mathrm{ext}} = 2.4\,\mathrm{A}$.

B. Experimental time series

In the experiment, we explore the same period-1 spiking regime as in the numerical simulations, when the oscillators are uncoupled. The coexistence of periodic and chaotic orbits is observed for intermediate values of the coupling strength σ_2 ($0.25 < \sigma_2 < 0.69$) when σ_1 is fixed to $\sigma_1 = 0.05$. Figure 8 shows typical time series of the coexisting regimes when initial conditions are randomly changed by switching on and off the power supply.

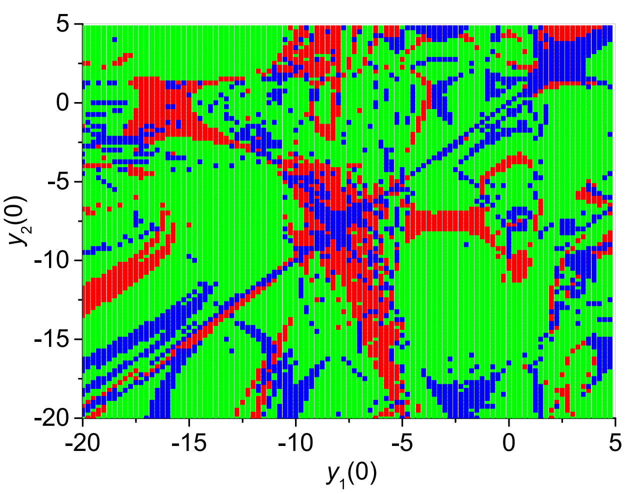

FIG. 6. Section of basins of attraction of coexisting periodic (green and red) and chaotic (blue) attractors shown in Figs. 2 and 3 for initial conditions $x_1(0) = -0.9221$, $z_1(0) = 1.2556$, $x_2(0) = -0.9127$, and $z_2(0) = 1.2603$.

C. Experimental bifurcation diagram

In order to compare the experimental results with the numerical ones, we fix the coupling strength to $\sigma_1 = 0.05$ in

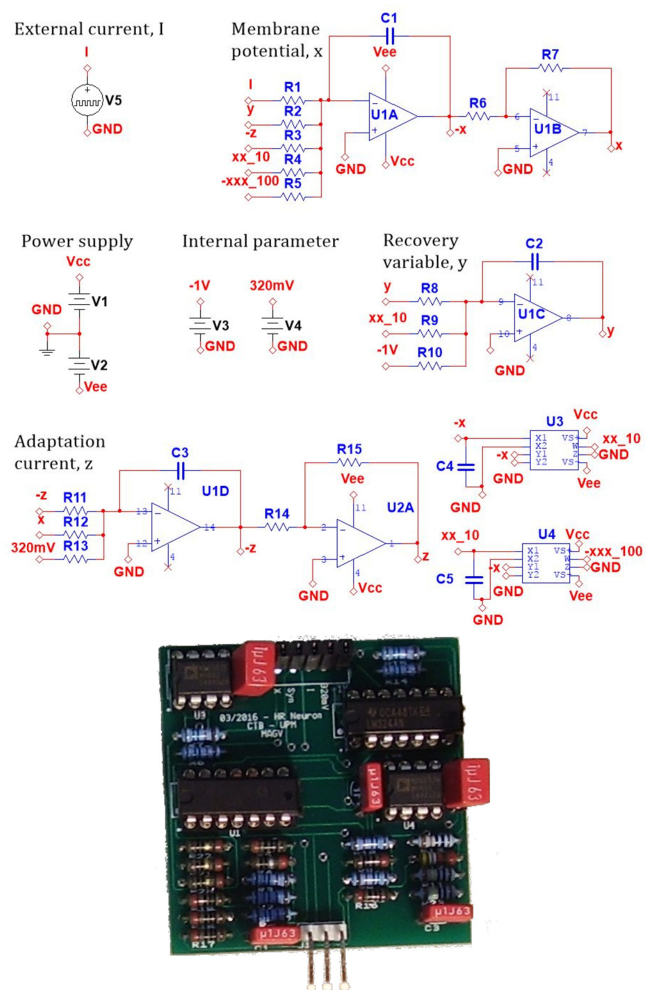

FIG. 7. Electronic scheme and general view of the electronic circuit based on the Hindmarsh-Rose model.

TABLE I. Hindmarsh-Rose circuit's electronic components.

Component	Value
R1, R2, R3, R4, R5, R6, R7, R8, R10, R14, R15	10 kΩ
R4	333 Ω
R5	100 Ω
R9	0.2 kΩ
R11	2 MΩ
R12	500 kΩ
R13	100 kΩ
C1, C2, C3	0.01 μF
C4, C5	1 μF
U1, U2	LM324AN
U3, U4	AD633AN
V1, V2	±15 V
V3	−1 V
V4	320 mV
V5	Voltage pulse
GND	Ground

one direction and use the coupling strength σ_2 in another direction as a control parameter. The resulting experimental bifurcation diagram of the normalized standard deviation (NSD) of the interspike interval (ISI) of the voltage V_{x2} is shown in Fig. 9.

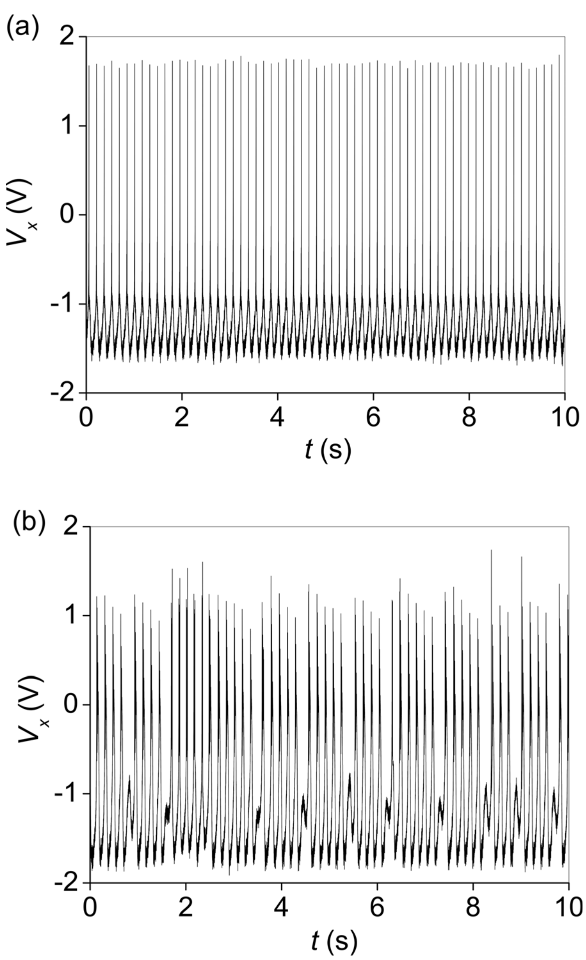

FIG. 8. Experimental time series of coexisting (a) periodic and (b) chaotic regimes for $\sigma_1 = 0.05$ and $\sigma_2 = 0.66$.

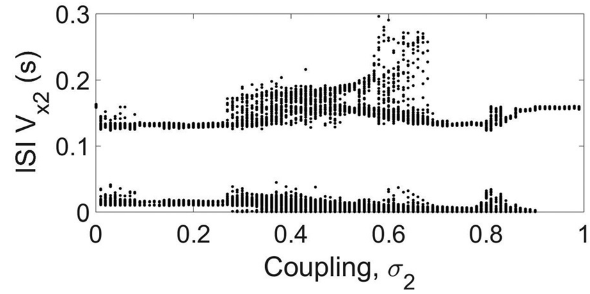

FIG. 9. Experimental bifurcation diagram of NSD of ISI of V_{x2} as a function of the coupling strength σ_2 at $\sigma_1 = 0.05$. Multistability emerges at intermediate coupling strengths.

D. Coherence

In a similar way to the numerical simulations, we experimentally measure the coherence of the coupled oscillators as standard deviation (SD) of the ISI of voltage V_x. The results of this study are presented in Fig. 10 with the bifurcation diagrams in the space of two coupling strengths. The larger the SD, the lower the coherence. One can see that at low couplings the system is weak coherent (less regular) compared to that for strong coupling (more regular). The asymmetry in the coherence with respect to the diagonal $\sigma_1 = \sigma_2$ is a signature of multistability. The difference between the diagrams of two electronic neurons indicates that they exhibit different dynamical behaviors even in the presence of experimental noise.

It should be noted that due to inevitable experimental noise, the experimental study of the multistable regimes is difficult because the system switches from time to time between different coexisting regimes, as shown in Fig. 11. Such windows of intermittency appear randomly in one of the neurons that often lead to their desynchronization.

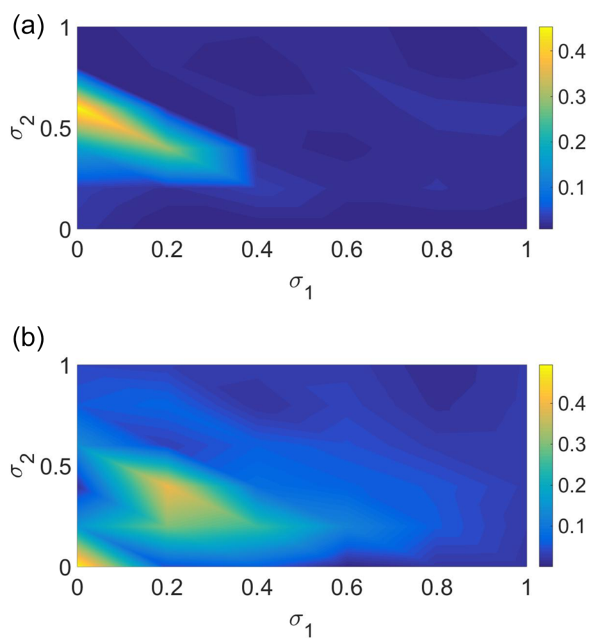

FIG. 10. Experimental standard deviation of ISI (in seconds) of (a) V_{x1} and (b) V_{x2} as a function of the coupling strengths. The asymmetry with respect to the diagonal indicates multistability.

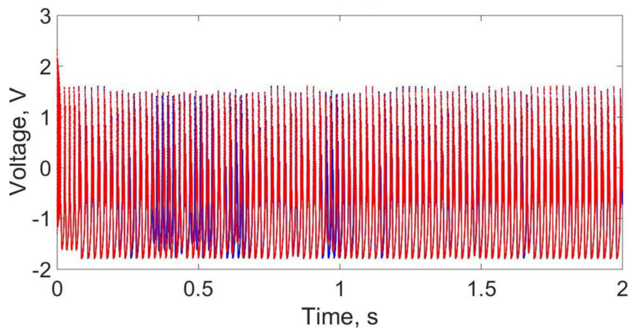

FIG. 11. Intermittent multistate synchronization. The time traces of two coupled neuronal oscillators are shown in red and blue.

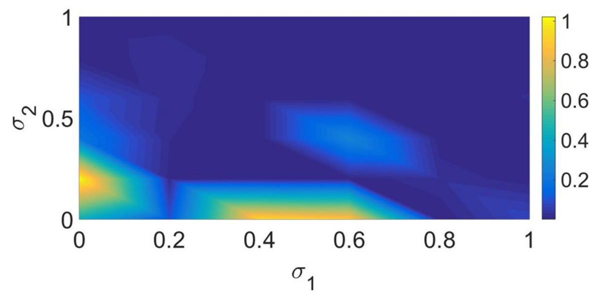

FIG. 12. Synchronization error E (in volts) as a function of the coupling strengths.

Weakly coupled neurons oscillate asynchronously, whereas for strong couplings they synchronize. Complete synchronization can be characterized by average error $E = \langle|V_{x2} - V_{x1}|\rangle$ between membrane potentials of the coupled neurons. In the intermittency regime, the synchronization error is high. In Fig. 12, we plot the normalized error in the space of the coupling strengths. One can see that the large error occurs for weak and intermediate coupling strengths, whereas for large coupling strengths $E = 0$ (blue color in the figure). The asymmetry in the error with respect to the diagonal is the consequence of multistability and multistate intermittency.

IV. CONCLUSION

In this paper, we have demonstrated that asymmetric electrical coupling can induce multistability in a coupled neural system. The coexistence of attractors emerges at relatively weak coupling strengths and depends on the asymmetry. In the Hindmarsh-Rose model of two coupled neuronal oscillators, we have found the coexistence of three attractors, two periodic and one chaotic. The multistability has been revealed through time series, phase portraits, bifurcation diagrams, coherence, Lyapunov exponents, and basins of attraction of the coexisting states. The coexistence of attractors was observed for relatively small coupling, whereas for very strong coupling, the system was monostable and completely synchronized.

In addition, in this paper, we have provided the experimental evidence of asymmetry-induced multistability using electronic circuits simulating dynamical behavior of coupled neurons. The experimental results are in a good agreement with the numerical ones. Due to experimental noise, multistate intermittency arose for certain coupling strengths.

The results of this paper can explain the appearance of different firing patterns in neurophysiological experiments. The existence of multistability due to asymmetric coupling and related effects, such as multistate intermittency due to inherent noise, should be taken into account by considering dynamics of complex neuronal networks.

ACKNOWLEDGMENTS

This work was supported by the Ministry of Economy and Competitiveness (Spain) (Project No. SAF2016-80240). The model development was supported by the Russian Science Foundation (Grant No. 16-12-10100).

[1]F. F. Bukauskas, A. B. Angele, V. K. Verselis, and M. V. L. Bennett, Proc. Natl. Acad. Sci. U.S.A. **99**, 7113 (2002).
[2]A. N. Pisarchik and U. Feudel, Phys. Rep. **540**, 167 (2014).
[3]E. Tognoli and J. A. Scott Kelso, Neuron **81**, 35 (2014).
[4]Y. A. Chen and T. R. Huang, Sci. Rep. **7**, 43313 (2017).
[5]W. Singer and C. M. Gra, Annu. Rev. Neurosci. **18**, 555 (1995).
[6]R. Ritz and T. J. Sejnowski, Curr. Opin. Neurobiol. **7**, 536 (1997).
[7]P. J. Uhlhaas and W. Singer, Neuron **52**, 155 (2006).
[8]A. N. Pisarchik, R. Jaimes-Reátegui, J. R. Villalobos-Salazar, J. H. Garcia-Lopez, and S. Boccaletti, Phys. Rev. Lett. **96**, 244102 (2006).
[9]S. Boccaletti, A. N. Pisarchik, C. I. del Genio, and A. Amann, *Synchronization: From Coupled Systems to Complex Networks* (Cambridge University Press, Cambridge, 2018).
[10]W. H. Evans and P. E. Martin, Mol. Membr. Biol. **19**, 121 (2002).
[11]M. V. L. Bennett and R. S. Zukin, Neuron **41**, 495 (2004).
[12]B. W. Connors, Neurobiology **77**, 610 (2017).
[13]J. Hounsgaard and I. Mintz, J. Physiol. **398**, 591–603 (1988).
[14]R. H. Lee and C. J. Heckman, J. Neurophysiol. **80**, 583–593 (1998).
[15]D. J. Bennett, Y. Li, and M. Siu, J. Neurophysiol. **86**, 1955–1971 (2001).
[16]H. Kim and K. E. Jones, J. Comput. Neurosci. **30**, 659 (2011).
[17]C. Morris and H. Lecar, Biophys. J. **35**, 193–213 (1981).
[18]V. Booth and J. Rinzel, J. Comput. Neurosci. **2**, 299–312 (1995).
[19]J. L. Hindmarsh and R. M. Rose, Proc. R. Soc. London, Ser. B **221**, 87 (1984).
[20]L. A. Hodgkin and A. F. Huxley, J. Physiol. **117**, 500 (1952).
[21]M. I. Rabinovich and H. D. I. Abarbanel, Neuroscience **87**, 5 (1998).
[22]I. Belykh, E. de Lange, and M. Hasler, Phys. Rev. Lett. **94**, 188101 (2005).
[23]I. Franović, K. Todorović, N. Vasović, and N. Burić, Chaos **21**, 033109 (2011).
[24]B. K. Bera, D. Ghosh, and T. Banerjee, Phys. Rev. E **94**, 012215 (2016).
[25]M. A. García-Vellisca, R. Jaimes-Reátegui, and A. N. Pisarchik, Math. Modell. Nat. Phenom. **12**, 43 (2017).
[26]H. D. I. Abarbanel, R. R. Huerta, and M. I. Rabinovich, Neural Comput. **8**, 1567 (1996).
[27]M. Bazhenov, R. Huerta, M. I. Rabinovich, and T. Sejnowski, Physica D **116**, 392 (1998).
[28]M. S. Baptista, F. M. M. Kakmeni, and C. C. Grebogi, Phys. Rev. E **82**, 036203 (2010).
[29]M. I. Rabinovich, H. D. I. Abarbanel, R. Huerta, R. Elson, and A. I. Selverston, IEEE Trans. Circuits Syst. **44**, 997 (1997).
[30]A. N. Pisarchik and R. Jaimes-Reátegui, Phys. Rev. E **92**, 050901(R) (2015).
[31]M. A. García-Vellisca, A. N. Pisarchik, and R. Jaimes-Reátegui, Phys. Rev. E **94**, 012218 (2016).